Hindawi
Advances in Materials Science and Engineering
Volume 2022, Article ID 9626824, 15 pages
https://doi.org/10.1155/2022/9626824

Research Article

A Novel Cold-Mixed Epoxy Concrete and Its Comparison with Hot-Mixed Epoxy Asphalt Concrete

Kuan Li,[1] **Jianguang Xie**,[1] **Youqiang Pan**,[2] **Yanping Liu**,[1] **and Zhanqi Wang**[1]

[1]*Department of Civil and Airport Engineering, Nanjing University of Aeronautics and Astronautics, Nanjing 211106, China*
[2]*Jiangsu Sinoroad Engineering Research Institute Co. Ltd., Nanjing 210000, China*

Correspondence should be addressed to Jianguang Xie; xiejg@nuaa.edu.cn

Received 2 June 2022; Revised 28 June 2022; Accepted 5 July 2022; Published 8 August 2022

Academic Editor: Minghui Gong

A novel cold-mix epoxy (CME) concrete was developed to meet the urgent demand of quick maintenance in long-span steel deck pavement. Considering that the CME is a thermosetting resin, a differential scanning calorimeter (DSC) was employed to evaluate the curing behavior of the CME binder. Dynamic mechanical analysis (DMA) was used to investigate the viscoelasticity of the CME binder. The semicircular bending test and the three-point bending test were used to evaluate the crack resistance of CME concrete. Long-term performance was investigated by comparing the fatigue behavior of the CME concrete and hot-mixed epoxy asphalt (HMEA) concrete. The results showed that the curing reaction order of CME is similar to that of HME (hot-mixed epoxy) and the activation energy of CME is slightly higher than that of HME which means that the reactivity of the latter is higher. The bimodality that occurs in tanδ curve means that there are two phases existing in the CME and HMEA microstructure, while the secondary phase ensures that the CME and HMEA have good damping behavior. CME concrete has a better crack resistance than HMEA concrete at low temperature, and a similar crack resistance compared with HMEA concrete at high temperature. From the residual ratio of flexural stiffness after 1 million load cycles, the CME concrete shows better fatigue resistance than the HMEA concrete.

1. Introduction

Due to the advantages of an orthotropic steel deck with lightweight, high strength, and fast construction, it has been widely used in the construction of long-span steel bridges in European countries, Japan, the United States, and other countries for more than 70 years [1]. The steel deck pavement technology was mainly investigated by European countries, the United States, and Japan began in the 1950s [2]. The United Kingdom mainly adopts monolayer stone mastic asphalt pavement, while Germany, the Netherlands, and Japan mainly adopt compound gussasphalt pavement [3], and the United States mainly adopts double layer epoxy asphalt pavement [4] due to the excellent fatigue resistance of the epoxy asphalt.

In the late 1950s, Shell developed epoxy asphalt (EPON-Epoxy Asphalt), which was first used as a coating on airport runways to improve impact resistance and durability [1, 5]. In 1967, the epoxy asphalt mixture was used to pave the orthotropic steel deck of the San Mateo-Hayward bridge in the United States for the first time [6]. In 2001, epoxy asphalt pavement was successfully used at the Nanjing Yangtze River Second Bridge [7], then epoxy asphalt pavement was widely used in the Chinese construction of long-span steel bridge [1]. Currently, epoxy asphalt pavement in China is more than $150 \times 104\,m^2$ [8].

As we know, epoxy asphalt is used in long-span steel deck pavement, including warm-mix epoxy asphalt (WMEA) and hot-mix epoxy asphalt (HMEA). WMEA provided by ChemCo System need to be mixed at 110–121°C and then cured at room temperature for above 30 days [9], while HMEA provided by Kindai Kasei need to be mixed at 165–190°C and then cured at room temperature for above 7 days [10].

Due to the steel plate of the steel deck bridge constructed in an early age was only 12 mm, fatigue cracks and pothole diseases appear in epoxy asphalt pavement after 5–10 years of use [11]. As a result, many epoxy asphalt pavements

constructed at an early age are in urgent need of maintenance and repair [12]. Long-span steel bridges are always in a traffic throat position, completely closed traffic for maintenance is almost impossible, and quick maintenance technology is urgent for long-span steel deck pavement. Obviously, WMEA and HMEA are all not suitable for the maintenance and repair of the epoxy asphalt pavement due to the high mixing temperature and long curing time.

In recent years, cold-mixed epoxy asphalt (CMEA) [13–15] developed in China was used on the Zhijiang River Bridge, Jiashao Bridge, Liaohe River Bridge, etc. The solvent asphalt, coal tar, etc. were used as toughening composition in CMEA, with the increase of service time, the toughening component gradually migrate out of the cured network, as a result, fatigue cracking and potholes diseases appeared in steel deck pavement rapidly.

In order to avoid the performance degradation caused by the migration of toughening composition, flexible chains were introduced into the molecular structure of cured epoxy resin by chemical grafting method, then a novel cold-mix epoxy(CME) with a simultaneous interpenetrating polymer network (IPN) was developed by our team [16].

The evaluation methods of steel deck pavement materials are relatively weak, and most of the methods are similar to common asphalt pavement [17]. Considering that epoxy asphalt is a typical thermosetting material, the DSC was used to evaluate the curing behavior of WMEA [18], HMEA [19, 20], and CMEA [15]. Further, modulated differential scanning calorimeter (MDSC) was used to investigate the reaction kinetics of epoxy asphalt [21]. DMA was used to evaluate the epoxy asphalt binder [19, 20, 22–24] and the epoxy asphalt concrete [25–27]. The fatigue behavior of epoxy asphalt is a hot topic on steel deck pavement, and the test method includes the three-point bending fatigue test [28] and the four-point bending fatigue test [11, 29, 30]. For epoxy asphalt, the tensile test is the main method of evaluating the mechanical properties, and the viscosity is the main method of evaluating reactivity [31]. For epoxy asphalt concrete, the Marshall test, freeze-thaw spitting test, wheel tracking test, and three-point bending test are the main methods to evaluate the basic mechanical performances. Due to WMEA, HMEA and CME are all viscoelastic materials, the static mechanical analysis is not enough to evaluate the key performances at different temperatures.

Considering this issue, CME and HMEA for steel deck pavement were evaluated comprehensively. In this study, DSC, tensile test, and DMA were used to analyze the CME binder and HMEA binder, then the Marshall test, freeze-thaw splitting test, wheel tracking test, three-point bending test, semicircular bending test, and four-point beam fatigue test were used to evaluate the CME concrete and HMEA concrete.

2. Experimental

2.1. Raw Materials

2.1.1. Binder. CME is a novel material provided by Jiangsu Sinoroad Transportation Science and Technology Co., Ltd. (Nanjing, China) for steel deck pavement. The CME is made up of the main agent (part A) and the curing agent (part B), and the weight ratio of part A to part B is 5 : 1. Part A is a mixture of bisphenol A type epoxy resin, and part B is a mixture of amine curing agent. Details of part A and part B are given in Tables 1 and 2.

HMEA is a normal material provided by Kindai Kasei Co., Ltd. (Aichi-ken, Japan) for steel deck pavement. HMEA is composed of the main agent (part A), the curing agent (part B), and the asphalt (part C), and the weight ratio of part A to part B is 56 : 44, the weight ratio of epoxy to asphalt is 50 : 50. Part A is a mixture of epoxy resin, part B is a mixture of amine curing agent, and part C is matrix asphalt (70# paving asphalt) obtained from Jiangsu Zhongyitong Road New Materials Co., Ltd. (Zhenjiang, China). Details of Part A, Part B, and Part C are given in Tables 3–5, respectively.

2.1.2. Aggregates and Mix Design. The basalt aggregates obtained from Jiangsu Maodi Group were used in the CME and HMEA mixtures. A typical dense gradation with a 13.2 mm nominal maximum size aggregate was used for the concrete testing, and the grading range and composite gradation are shown in Figure 1. The mass ratio of various mineral materials is as follows: 1# (4.75–9.5 mm): 2# (2.36–4.75 mm): 3# (0.6–2.36 mm): 4# (0–0.6 mm): limestone mineral powder = 25 : 21.5 : 22 : 23 : 8.5. The binder-aggregate ratio of the CME and HMEA mixtures was 7.5% and 6.5%, respectively.

2.2. Sample Preparation

2.2.1. CME Concrete Preparation. The mixture of part A and part B was stirred evenly in a certain proportion, until a homogeneous CME mixture was observed. The CME mixture was immediately poured into cold aggregates, then the CME mixture was mixed with a forced concrete mixer, until a homogeneous mixture was observed. Marshall samples were prepared according to ASTM *D* 6926, and rutting samples were prepared according to EN 12697–33. All samples were treated at 60°C for 16 h and then naturally cooled for 24 h before performing the relevant performance tests.

2.2.2. HMEA Concrete Preparation. Parts A and B were preheated at 60°C in an oven for 2 h, and part C was preheated at 160°C in an oven for 4 h. After preheating, the mixture of parts A and B (hot-mix epoxy, HME) was stirred evenly in a certain proportion, then a certain proportion of part C was added into the HME with continuous mechanical stirring, until a homogeneous mixture (hot-mix epoxy asphalt, HMEA) was observed. The HMEA was immediately poured into hot aggregates, and then the HMEA mixtures were mixed with a forced concrete mixer, until a homogeneous mixture was observed. Marshall samples were prepared according to ASTM *D* 6926, and rutting samples were prepared according to EN 12697–33. All samples were treated at 60°C for 4 d and then naturally cooled for 24 h before performing relevant performance tests.

Table 1: Properties of part A in CME.

Property	Value	Method
Viscosity at 23°C (mPa s)	4000–8000	ASTM D445
Specific gravity at 23°C (g/ml)	1.0–1.2	ASTM D1475
Appearance	Colorless transparent liquid	Visual

Table 2: Properties of part B in CME.

Property	Value	Method
Viscosity at 23°C (mPa·s)	20–200	ASTM D445
Specific gravity at 23°C (g/ml)	0.8–1.0	ASTM D1475
Appearance	Light brown transparent liquid	Visual

Table 3: Properties of part A in HMEA.

Property	Value	Method
Viscosity at 23°C (mPa s)	1000–5000	ASTM D445
Specific gravity at 23°C (g/ml)	1.0–1.2	ASTM D1475
Appearance	Straw color transparent liquid	Visual

Table 4: Properties of part B in HMEA.

Property	Value	Method
Viscosity at 23°C (mPa s)	100–800	ASTM D445
Specific gravity at 23°C (g/ml)	0.8–1.0	ASTM D1475
Appearance	Light cinnamon color liquid	Visual

Table 5: Properties of part C in HMEA.

Property	Value	Method
Penetration at 25°C (0.1 mm)	63.0	JTG E20, T0604
Softening point (°C)	48.5	JTG E20, T0606
Ductility at 15°C (cm)	>200	JTG E20, T0605
Density at 15°C (g/ml)	1.035	JTG E20, T0603
Viscosity at 60°C (Pa s)	173	JTG E20, T0625
Wax contain (%)	1.83	JTG E20, T0615

2.3. Characterization

2.3.1. Differential Scanning Calorimeter (DSC). The curing kinetics of CME and HMEA were measured with DSC 214 Polyma (Netzsch, Germany) under a nitrogen flow of 20 ml/min. Approximately 10 mg of sample was tested with a temperature range of RT to 250°C at a heat rate of 5°C/min, 10°C/min, 15°C/min, and 20°C/min, respectively.

According to the Kissinger model, the activation energy can be obtained from

$$\mathrm{d}\frac{\left[\ln\left(\beta/T_p^2\right)\right]}{d\left(1/T_p\right)} = -\frac{E_a}{R}, \tag{1}$$

where T_p is the peak temperature of the exothermic peak, β is the constant heat rate, E_a is the activation energy of the curing reaction, and R is the universal gas constant. The value of E_a can be obtained by plotting $\ln(\beta/T_p^2)$ versus $1/T_p$.

According to the Crane model, the curing reaction order can be obtained from:

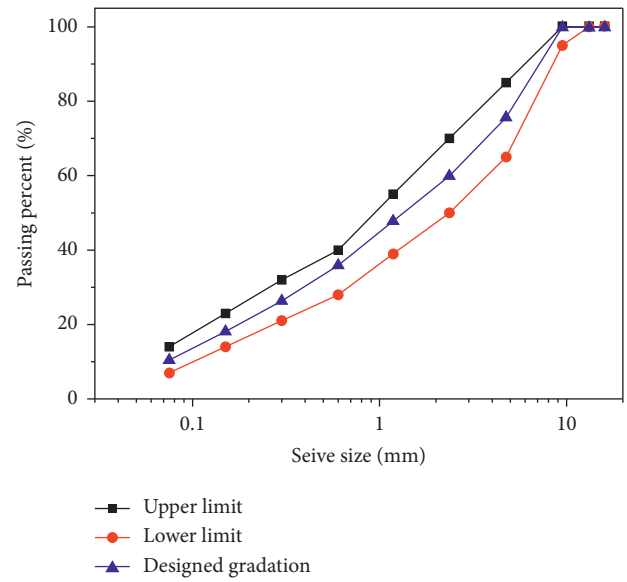

Figure 1: Aggregate gradation curve.

$$\mathrm{d}\frac{[\ln\beta]}{d\left(1/T_p\right)} = -\frac{E_a}{nR}, \tag{2}$$

where T_p is the peak temperature of the exothermic peak, β is the constant heat rate, Ea is the activation energy of the curing reaction, R is the universal gas constant, and n is the curing reaction order. The value of n can be obtained by plotting $\ln\beta$ versus $1/T_p$.

2.3.2. Tensile Test. The tensile properties of the CME, HME, and HMEA binders were performed on a tensile testing machine (QJ211S, Shanghai Qingji Instruments and Apparatus Technology Co., Ltd) according to ASTM D638. Due to the difference in the modulus of different kinds of binders, type IV specimens were used for the tensile properties test [32]. All specimens were placed at $23 \pm 1^{\circ}C$ for 24 h before being tested, and the tensile rate was 50 mm/min.

2.3.3. Dynamic Mechanical Analysis (DMA). The DMA was performed on a Diamond DMA (Perkin Elmer Instruments, USA) according to ASTM D7028. The specimen length is 4 ± 0.2 mm, width is 4 ± 0.2 mm, and thickness is 2 ± 0.2 mm. The measurements were taken in tension mode, the tensile strain was constant at 0.1%, and the frequency was constant at 1 Hz. All specimens were heated from $-80^{\circ}C$ to $80^{\circ}C$ with a heating rate of $2^{\circ}C$/min. High purity nitrogen gas was used to protect the samples from oxidation during heating and the flow rate was constant at 100 ml/min.

2.3.4. Marshall Test. The Marshall test was carried out on an asphalt mixture stability tester (DF-100K, Nanjing Tuoxing Instrument Research Institute) according to JTG E20 T0709.

2.3.5. Freeze-Thaw Splitting Test. The freeze-thaw splitting test was carried out on an asphalt mixture stability tester (DF-100K, Nanjing Tuoxing Instrument Research Institute) according to JTG E20 T0716.

2.3.6. Wheel Tracking Test. The wheel tracking test was carried out on an automatic rutting tester (HYCZ-5C, Beijing Aerospace Measurement and Control Technology Research Institute) according to JTG E20 T0719.

2.3.7. Three-Point Bending Test. The three-point bending test was carried out on a servohydraulic dynamic testing system (DTS-30, Pavetest, Italy) according to JTG E20 T0715. All specimens with $(250 \pm 2\,\text{mm}) \times (30 \pm 2\,\text{mm}) \times (35 \pm 2\,\text{mm})$ were cut from the rutting plate using an automatic pave saw (APS, Matest, Italy). All samples were placed at $15^{\circ}C$ or $-10^{\circ}C$ for 2 h before being tested and the loading rate was 50 mm/min. The load versus displacement curves were recorded during the measurement and the impact toughness [33] was obtained by integrating the load versus displacement curve.

2.3.8. Semicircular Bending Test (SCB). The fracture potential of CME concrete and HMEA concrete was performed on a servohydraulic dynamic testing system (DTS-30, Pavetest, Italy) according to AASHTO TP124. Samples with $(\Phi 150 \pm 1\,\text{mm}) \times (50 \pm 1\,\text{mm})$ were prepared from a rotating compaction sample. Cut a notch along the symmetry axis of each semicircular specimen to a depth of 15 ± 1 mm and 1.5 ± 0.1 mm in width. Figure 2 shows the test fixture and specimen configuration of the SCB test. The test is carried out using displacement control at a rate of 50 mm/min. The test stops when the load drops below 0.1 kN.

2.3.9. Four-Point Beam Fatigue Test. The fatigue life and failure energy determined by the four-point beam fatigue test were extensively used to estimate the fatigue life of the steel deck pavement layers under repeated traffic loading [11, 29, 30]. The curves of stiffness modulus, phase angle, and accumulated energy consumption against the number of load cycles were obtained by a stand-alone servo-pneumatic four-point beam system (Pavetest, Italy) according to AASHTO T321. Fatigue damage theory and stress mode of orthotropic steel bridge deck pavement determine that fatigue endurance limit is an important parameter to reflect the fatigue performance of the pavement layer [11]. Therefore, the testing was conducted under a strain control mode, with a half sinusoidal load at a frequency of 10 Hz. Figure 3 shows the test fixture and loading diagram of the four-point beam fatigue test. The test was terminated after 1,000,000 load cycles or the stiffness modulus was reduced to 50% of the initial stiffness modulus. Before four-point beam fatigue measurement, all specimens $(380 \pm 6\,\text{mm}) \times (63 \pm 6\,\text{mm}) \times (50 \pm 6\,\text{mm})$ should be in insulation under $15^{\circ}C$ for 24 h.

3. Results and Discussion

3.1. Curing Behavior. DSC is widely used to estimate the curing behavior of thermosetting resin, especially epoxy resin [18]. Figure 4 shows the non-isothermal curing behavior of CME and HME by curing the sample with different heating rates. Obviously, with the heating rate increasing from $5^{\circ}C$/min to $20^{\circ}C$/min the exothermic peak gradually shifted to the high-temperature region and the area of the exothermic peak gradually increased. In general, the exothermic process of CME is relatively flat, while the exothermic process of HME is relatively concentrated.

The initial temperature (TI), the peak temperature (TP), and the final temperature (TF) of the exothermic peak can be easily obtained by DSC analysis software. For the CME binder, when the heating rate increases from $5^{\circ}C$/min to $20^{\circ}C$/min, TI increases from $51.7^{\circ}C$ to $67.4^{\circ}C$, TP increases from $91.4^{\circ}C$ to $121.2^{\circ}C$, and TF increases from $120.8^{\circ}C$ to $152.5^{\circ}C$. Similarly, for the HME binder, when the heating rate increases from $5^{\circ}C$/min to $20^{\circ}C$/min, Ti increases from $44.0^{\circ}C$ to $54.6^{\circ}C$, TP increases from $114.0^{\circ}C$ to $150.1^{\circ}C$, and Tf increases from $181.4^{\circ}C$ to $250.0^{\circ}C$.

To calculate the E_a value of CME and HME, we take $1/T_p$ as the coordinate x and $\ln(\beta/T_p^2)$ as the coordinate y, and then the scatter diagram is fitted by linear function as shown in Figure 5. According to the Kissinger model, E_a of CME and HME can be calculated as 48.85 kJ/mol and 45.76 kJ/mol as shown in Table 6. According to the Crane model, the value of n can be obtained by plotting $\ln\beta$ versus $1/T_p$ as shown in Figure 6. The slope of the fitting curve can be used to calculate the value of n, and n of CME and HME are 0.88 and 0.87 as shown in Table 6.

The activation energy (E_a) reflects the difficulty of the chemical reaction, the higher the E_a, the harder the reaction.

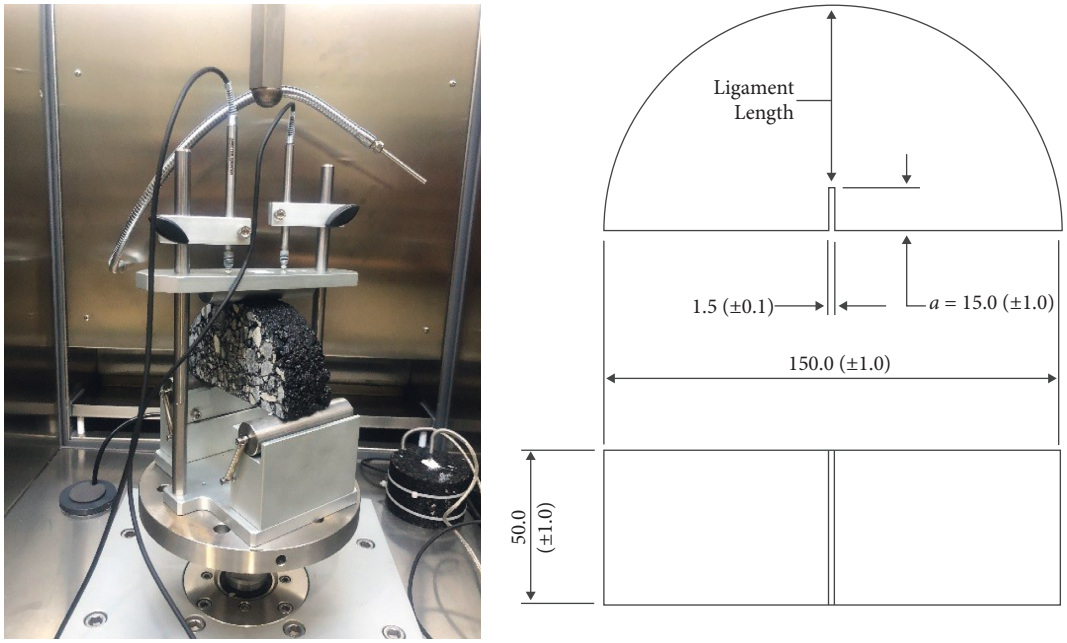

(a) (b)

Figure 2: (a) SCB test fixture and (b) SCB test specimen configuration (dimensions in millimeters).

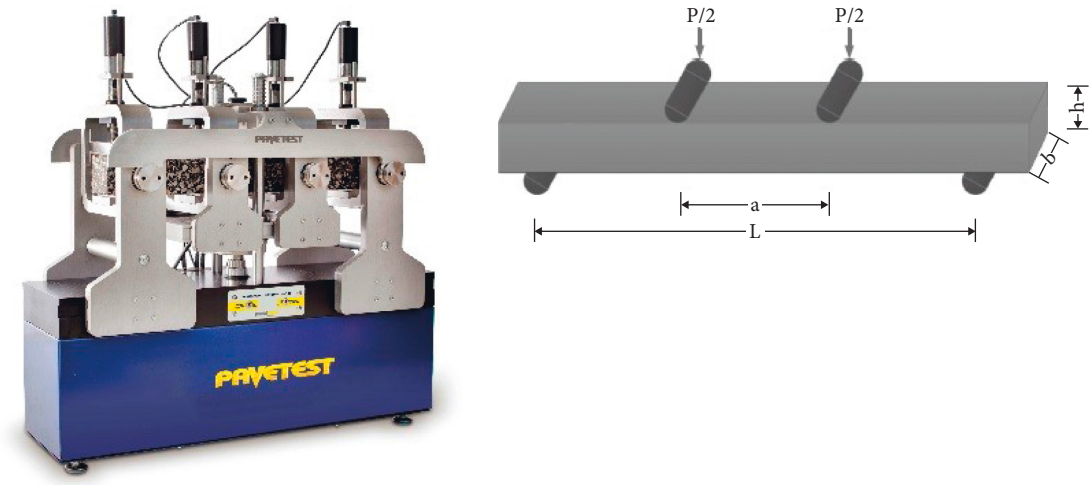

(a) (b)

Figure 3: (a) Four-point beam fatigue test fixture and (b) illustration of fatigue test.

HME reaction more easily as a result of the E_a of the CME higher than that of HME. Although HME is generally used under 170°C, but it can also be cured at room temperature. The curing reaction order (n) reflects the complexity of the chemical reaction. Because the curing agent of CME and HME are amine, the curing reaction order of CME is similar to HME.

3.2. Tensile Properties. As the operation is simple, the tensile test is widely used to evaluate the mechanical properties of the binder used in steel deck pavement. In the standard of JTG/T 3364–02 and GB/T 30598, tensile properties were used to assess the epoxy asphalt binder. In this paper, the tensile properties of CME, HME, and HMEA were compared. As shown in Figure 7, the tensile strength of CME, HME, and HMEA are 2.9 MPa, 6.2 MPa, and 2.7 Mpa, respectively, the elongation at break of CME, HME, and HMEA is 223%, 167%, and 208%, respectively.

According to the standard of JTG/T 3364–02, the tensile properties of epoxy asphalt used in steel deck pavement should meet the requirements given in Table 7. Obviously, for different kinds of epoxy asphalt used in steel deck pavement, its tensile performance requirements are also

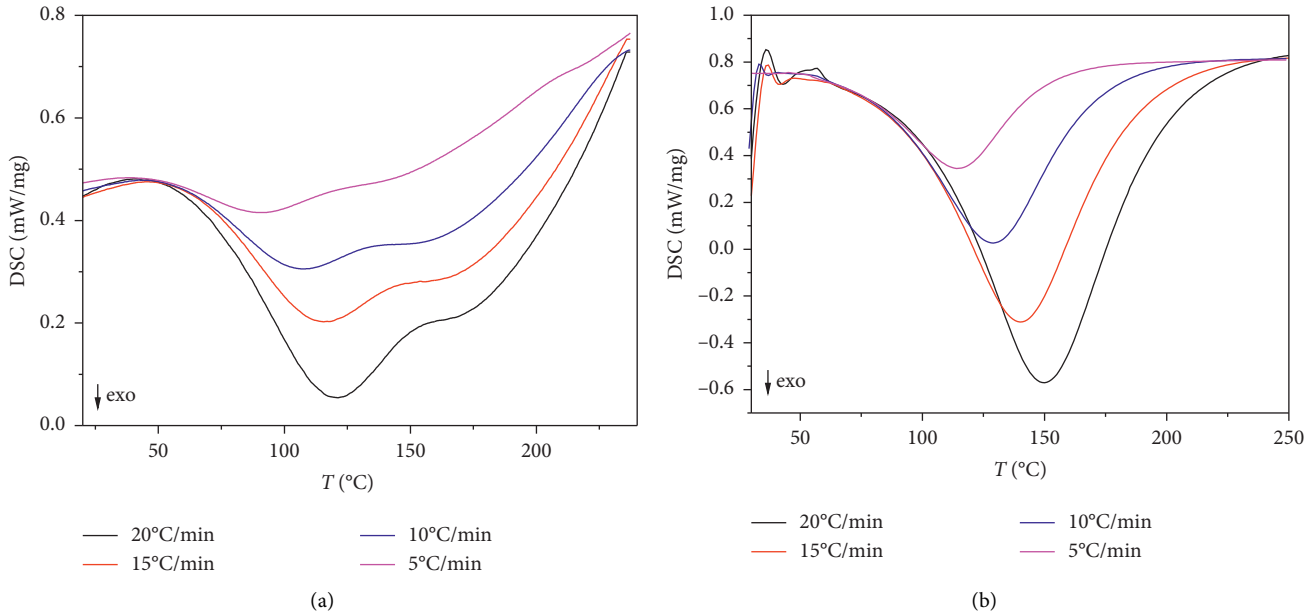

Figure 4: DSC curves of (a) CME and (b) HME with different heating rates.

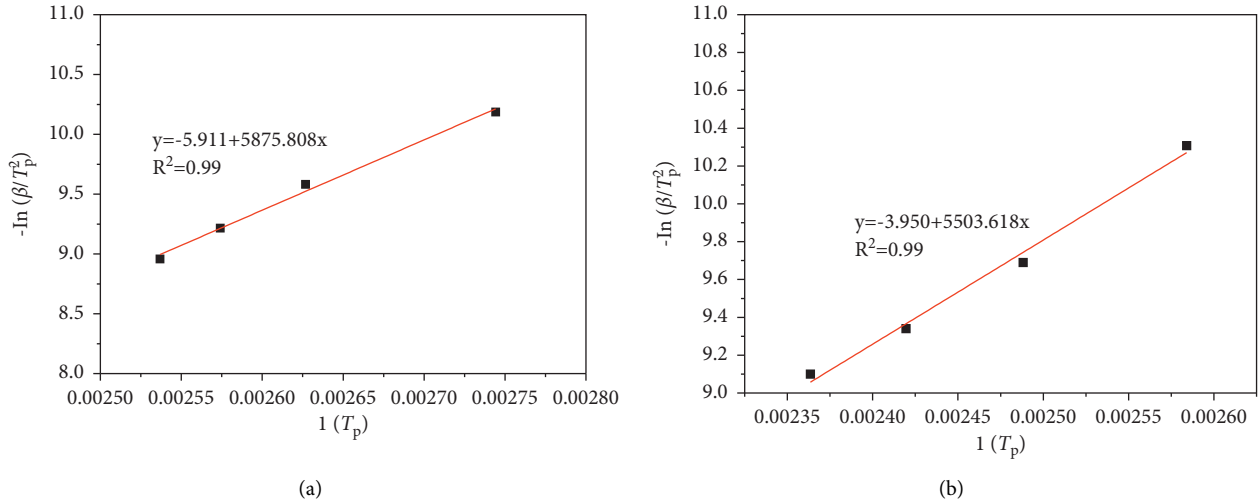

Figure 5: Fitting the curing curves of (a) CME and (b) HME based on the Kissinger equation.

Table 6: Curing behavior of the CME and HME by differential scanning calorimeter.

Type	Heating rate (°C/min)	T_i (°C)	T_p (°C)	T_f (°C)	E_a (kJ/mol)	n
CME	5	51.7	91.4	120.8	48.85	0.88
	10	62.3	107.7	135.1		
	15	65.8	115.5	147.2		
	20	67.4	121.2	152.5		
HME	5	44.0	114.0	181.4	45.76	0.87
	10	43.6	128.9	221.9		
	15	48.1	140.3	243.3		
	20	54.6	150.1	250.0		

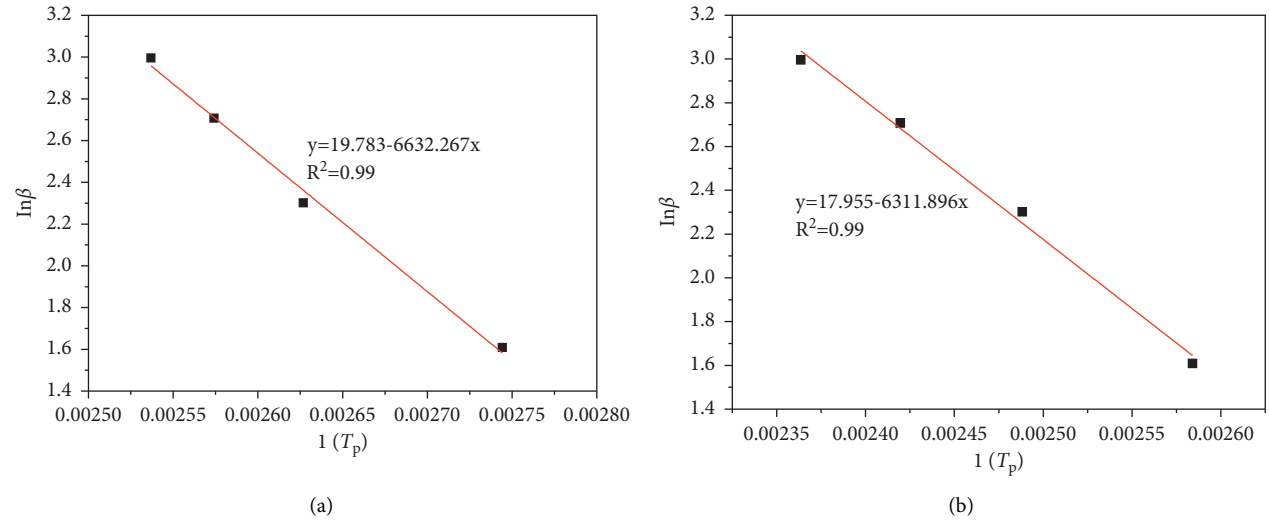

(a) (b)

Figure 6: Fitting the curing curves of (a) CME and (b) HME based on the Crane equation.

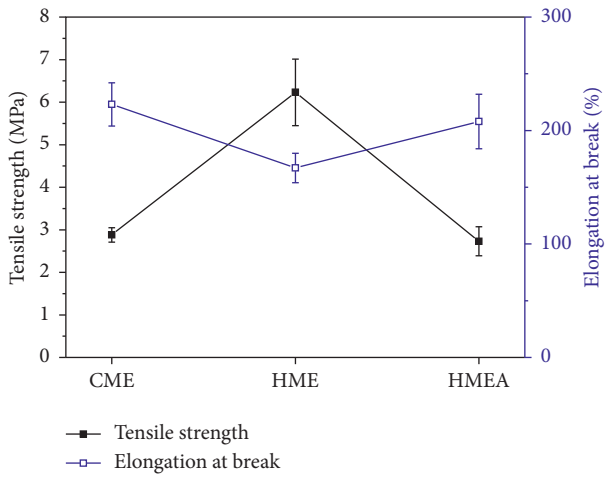

Figure 7: Tensile properties of the CME, HME, and HMEA.

different, which means that the tensile properties between different types of epoxy asphalt are not comparative. Actually, the tensile properties of the epoxy asphalt products are much higher than those requirements given in Table 7.

3.3. Damping Behavior. Given that there are many kinds of epoxy binder suitable for steel deck pavement and the tensile properties requirements are various for different kinds of epoxy binder, in this paper, DMA was employed to analyze epoxy-based binder used in steel deck pavement, and trying to find a comprehensive evaluation to epoxy-based binder. DMA is widely used to evaluate the viscoelastic properties of polymer materials [34]. Recently, DMA such as dynamic shear rheometer (DSR) is very popular in asphalt research [35, 36].

For viscoelastic materials, the peak of tanδ curve always represents different chain structure transitions. When tanδ is the biggest, the corresponding temperature is described as the glass transition temperature (T_g), and the second peak represents the secondary transition. As shown in Figure 8, there are two peaks in tanδ curve of CME, Peak 1 represents glass transition and Tg is 47.7°C, Peak 2 represents secondary transition and the corresponding temperature is −37.3°C. Two tanδ peaks that exist in tanδ curve mean that there are two phases existed in the CME microstructure. For HME, there is only one peak in tanδ curve, and T_g is 30.9°C. When 50% HME mixed with 50% asphalt, the peak belongs to HME appeared at 34.3°C, and the peak belongs to asphalt appeared at −43.1°C.

As shown in Figure 8, the storage modulus(E′) and the consumption modulus(E″) are all decreased with the increase of temperature for CME, HME, and HMEA, and the drop rate of modulus reaches to a maximum value when the temperature close to T_g. For CME, HME and HMEA, E″ is always less than E′, but when the temperature close to T_g, the value of E″ is close to the value of E′.

The damping behavior of CME, HME, and HMEA can be quantitatively evaluated by the maximum value of tanδ((tanδ)max), the temperature range for efficient damping (tanδ >0.3), and the area under the tanδ versus temperature curve [19, 37, 38]. The E′ of all specimens drops to less than 1 MPa when the temperature is above 75°C, as a result, the deformation of the specimen obstacle the testing. The various parameters on the damping behavior of the CME, HME, and HMEA by DMA are shown in Table 8. For CME, the minimum temperature for efficient damping is 22.7°C, the maximum temperature for efficient damping is above 75°C, and the temperature range for efficient damping is above 52.3°C, the integral of tanδ curve between −10°C and 70°C is 36.43. For HME, the temperature range for efficient damping is 41.6°C, the integral of tanδ curve between −10°C and 70°C is 33.52. For HMEA, the minimum temperature for efficient damping is 5.2°C, the maximum temperature for efficient damping is above 75°C, and the temperature range for efficient damping is above 69.8°C, the integrals of tanδ curve

Table 7: Technical requirements of epoxy asphalt in JTG/T3364-02.

Item	Hot-mix epoxy asphalt	Warm-mix epoxy asphalt	Cold-mix epoxy asphalt
Tensile strength (MPa)@23°C	≥2.0	≥1.5	≥2.0
Elongation at break (%)@23°C	≥100	≥200	≥50

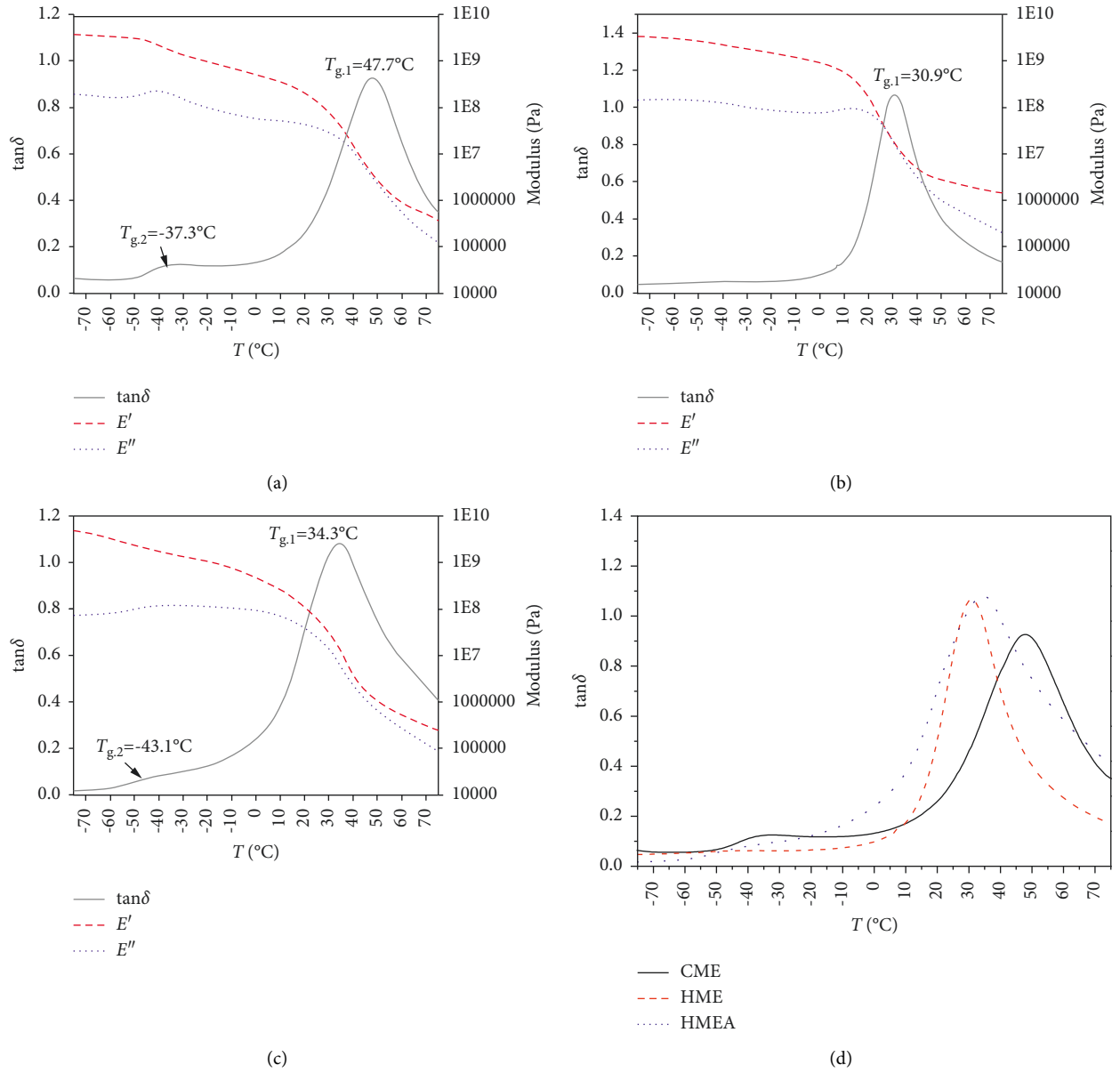

Figure 8: Dynamic mechanical properties of (a) CME, (b) HME, (c) HMEA, and (d) the comparison of tanδ.

between −10°C and 70°C is 49.75. Obviously, the damping behavior of CME, HME, and HMEA can be sorted in the following order: HMEA > CME > HME.

3.4. Workable Performance. Workable performance is very important for steel deck pavement due to the construction site is usually more than an hour's drive from the mixing station [4]. In the field of steel deck pavement, latency time is defined as the time from the beginning of epoxy-based concrete mixing to the completion of paving and rolling. Epoxy-based concrete is composed of reactive epoxy resin and aggregates. The curing reaction begins after mixing epoxy resin, and the viscosity gradually rises. The compacticity of epoxy-based concrete decreases gradually with the increase of latency time, and the adhesion between aggregate particles also decreases gradually. In this paper, the change in the void fraction and Marshall stability of Marshall

specimens with different latency times under the same compaction process are selected to evaluate the construction time of epoxy-based concrete.

For CME concrete, all of the samples were prepared at room temperature, and the air temperature (Tair) and the temperature of CME concrete (Tconcrete) were recorded during the preparation of CME concrete. As shown in Table 9, with the increase of latency time, Tconcrete rises gradually due to the exothermic reaction of CME, but the void fraction and Marshall stability do not change significantly. For HMEA concrete, all of the specimens were prepared at 170°C to 180°C, and the temperature of HMEA concrete (Tconcrete) was recorded during the preparation of HMEA concrete. As shown in Table 10, with increasing latency time, Tconcrete and the void fraction do not change significantly, but the Marshall stability decreases slowly, especially when the latency time is higher than 3 h.

For the two kinds of epoxy-based concrete, the Marshall stability shows different changing rules with latency time. For CME concrete, it has a slow reaction rate at room temperature. Even if the latency time reaches 4 h, it still has good compactability. The CME on the surface of adjacent aggregates can still react with each other and eventually form a high-strength matrix. Under 170°C~180°C, the reaction rate of HMEA is faster, but the degree of increase in viscosity of HMEA at high temperature is low, so even when the latency time reaches 4 h, the void fraction of HMEA concrete still does not change significantly. With the increase of latency time, the number of reactable epoxy groups on adjacent aggregates' surface decreases greatly, resulting in the decrease of the bond between adjacent aggregates, and finally, the Marshall stability of HMEA concrete decreases gradually with the increase of latency time. If it takes no more than a 10% drop in Marshall stability as the evaluation standard, the CME concrete's allowed latency time is more than 4 h while the HMEA concrete's allowed latency time is within 3 h. CME concrete and HMEA concrete meet the workable demands of actual construction.

3.5. Marshall Stability. The Marshall test results for CME concrete and HMEA concrete are given in Table 11. For CME concrete, the stability and flow values are 65.41 kN and 2.572 mm, and the residual stability ratio is 96.7% after the Marshall samples were immersed in 60°C water for 48 h. The Marshall stability of HME concrete is above 99.99 kN, and the addition of asphalt decreases the Marshall stability to 82.73 kN. Similarly, as discussed in 3.2, the addition of asphalt decreases the tensile strength from 6.2 MPa to 2.7 MPa. The residual ratios of CME concrete and HMEA concrete are all above 90%, which means that these concretes possess good resistance to water damage.

3.6. Water Damage Resistance. The freeze-thaw splitting test was used to assess the resistance to water damage of CME concrete and HMEA concrete. As shown in Table 12, the spitting strength of the CME concrete before and after freeze-thaw is 3.56 MPa and 3.27 MPa, respectively, and the residual ratio is 91.9%. The spitting strength of the HMEA concrete before and after freeze-thaw is 4.26 MPa and 4.09 MPa, respectively, and the residual ratio is 96.0%. According to the standard of JTG/T 3364–02, the residual ratio of epoxy asphalt concrete is required above 80%, which means that the concrete made from CME or HMEA binder show an excellent water damage resistance.

3.7. Rutting Resistance. The wheel tracking test with a solid rubber-faced tire is often used to provide the permanent deformation (rutting) evolution with the repetitions of loading. As shown in Table 13, the dynamic stability of CME concrete and HMEA concrete are 17328 cycles/mm and 14497 cycles/mm, respectively. The standard of JTG/T3364-02 requires that the dynamic stability is greater than 6000 cycles/mm, which means that CME concrete and HMEA concrete all have a good rutting resistance performance.

3.8. Crack Resistance. The three-point bending test is a traditional method to estimate the crack resistance of asphalt concrete, and the flexural modulus, maximum flexural strength, and maximum flexural strain are usually used to quantitatively estimate the low-temperature properties of asphalt concrete. In this paper, the load versus deflection curves at different temperatures were treated by integral, and the area of the load versus deflection curve was defined as impact toughness.

Although the tensile strength of the CME binder is similar to that of the HMEA binder, the flexural modulus of the CME concrete is less than that of the HMEA concrete, and the flexural modulus of the CME concrete is about half that of the HMEA concrete at both −10°C and 15°C as shown in Figure 9. Results of the three-point bending test of CME and HMEA concrete are shown in Table 14. When the testing temperature is −10°C, the maximum flexural strain of CME concrete is 7193 micro, and the maximum flexural strain of HMEA concrete is only 4152 micro. The impact toughness of CME concrete and HMEA concrete is 2900 N mm and 1987 N mm at −10°C, respectively, which means that the CME concrete has a better crack resistance than HMEA concrete at low temperature. The impact toughness of CME concrete is similar to HMEA concrete at 15°C, which means that those two concretes have similar crack resistance.

In this paper, semicircular bending test (SCB) was used to determine the crack resistance parameters of CME or HMEA concrete at 25°C and 60°C. As shown in Figure 10, the peak load and ultimate displacement of CME concrete are similar to HMEA concrete. When the testing temperature increased from 25°C to 60°C, the peak load of CME concrete decreased from 11.581 kN to 3.589 kN rapidly, and the peak load of HMEA concrete also decreased from 11.352 kN to 3.328 kN rapidly. Figure 11 shows photos of various samples after SCB testing.

The calculated fracture energy indicates the mixture's overall capacity of the mixture to resist cracking-related damage. The work of fracture (W_f) is calculated as the area under the load versus displacement curve. The fracture energy (G_f) is calculated by dividing the work of fracture

Table 8: Damping behavior of CME, HME, and HMEA determined by DMA.

Item	CME	HME	HMEA
Glass transition temperature, T_g (°C)	$T_{g,1} = 47.7$ $T_{g,2} = -37.3$	$T_{g,1} = 30.9$	$T_{g,1} = 34.3$ $T_{g,2} = -43.1$
Tanδ max	0.93	1.07	1.08
Temperature range of tanδ >0.3, (°C)	Min = 22.7, Max >75	Min = 15.8, Max = 57.4	Min = 5.2, Max >75
Integrals of tanδ curve between −10°C and 70°C	36.43	33.52	49.75

Table 9: Workable performance of CME concrete at room temperature.

Latency time (h)	Tair (°C)	Tconcrete (°C)	Void fraction (%)	Marshall stability (kN)
0.5	23.6	25.4	1.794	65.1
1.0	24.2	25.2	1.349	64.5
1.5	24.1	25.1	1.693	62.8
2.0	22.0	24.0	2.033	58.5
2.5	26.0	33.2	1.060	62.9
3.0	26.0	35.6	1.769	59.6
3.5	26.0	39.0	1.103	61.5
4.0	24.0	36.0	1.416	60.6

Table 10: Workable performance of HMEA concrete at 170°C.

Latency time (h)	Tconcrete (°C)	Void fraction (%)	Marshall stability (kN)
0.5	173.4	1.106	81.2
1.0	174.2	1.159	82.7
1.5	176.2	1.148	79.3
2.0	169.8	1.172	79.4
2.5	173.2	1.212	80.9
3.0	175.1	1.252	77.4
3.5	171.1	1.120	65.3
4.0	177.9	1.129	61.2

Table 11: Marshall test results of CME, HME, and HMEA concretes.

Type	60°C, 0.5 h		60°C, 48 h		Residual ratio (%)
	Stability (kN)	Flow value (0.1 mm)	Stability (kN)	Flow value (0.1 mm)	
CME concrete	65.41	25.72	63.24	25.23	96.7
HME concrete	>99.99	—	>99.99	—	—
HMEA concrete	82.73	26.30	81.98	25.74	99.1

Table 12: Freeze-thaw splitting test results of CME and HMEA concretes.

Type	Splitting strength (MPa)		Residual ratio (%)
	No freezing-thawing cycle	Freezing-thawing cycle	
CME concrete	3.56	3.27	91.9
HMEA concrete	4.26	4.09	96.0

Table 13: Wheel tracking test results of CME and HMEA concretes.

Type	Dynamic stability (cycles/mm)
CME concrete	17328
HMEA concrete	14497

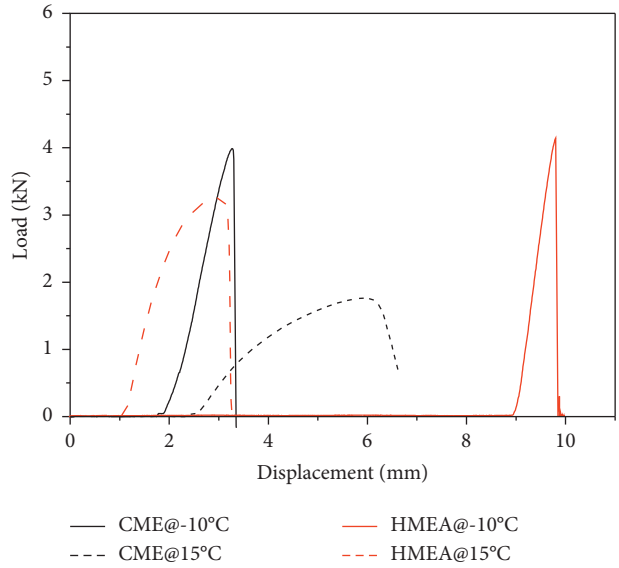

Figure 9: Load-displacement curves of the three-point bending test.

Table 14: The three-point bending test results of CME and HMEA concrete.

Temperature	Parameter	CME concrete	HMEA concrete
−10°C	Flexural modulus (MPa)	4529	8796
	Maximum flexural strength (MPa)	32.6	36.5
	Maximum flexural strain (micro)	7193	4152
	Impact toughness (N·mm)	2900	1987
15°C	Flexural modulus (MPa)	800	2619
	Maximum flexural strength (MPa)	14.4	27.3
	Maximum flexural strain (micro)	17955	10439
	Impact toughness (N·mm)	4978	4971

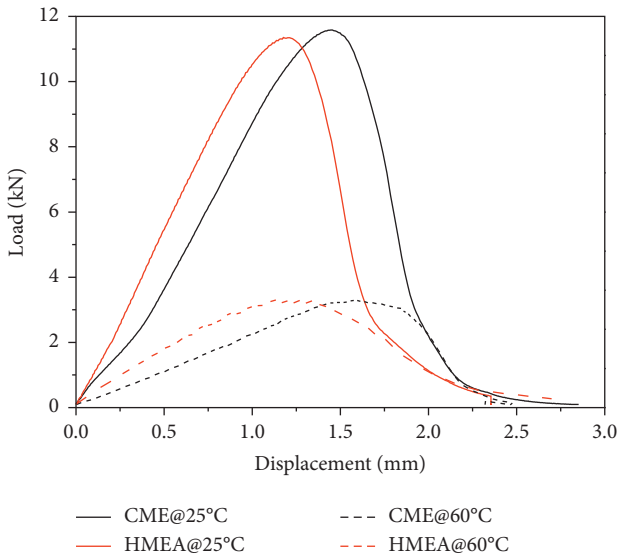

Figure 10: Load versus displacement curves of SCB.

(W_f) by the ligament area (the product of the ligament length and the thickness of the specimen) of the SCB specimen prior to testing.

$$G_f = \frac{W_f}{\text{Area}_{\text{lig}}} \times 10^6, \tag{3}$$

where G_f is fracture energy (J/m^2), W_f is work of fracture (J), and Arealig is ligament area (mm^2).

As shown in Table 15, the G_f at 25°C of CME concrete and HMEA concrete are 2068 J/m^2 and 2273 J/m^2, respectively, the G_f at 60°C of CME concrete and HMEA concrete are 888 J/m^2 and 952 J/m^2, respectively. Generally, a concrete with higher fracture energy can resist greater stresses with higher damage resistance, so CME concrete has a similar crack resistance compared to HMEA concrete.

3.9. Fatigue Resistance. The four-point beam fatigue test is suitable for estimating the steel deck pavement materials because its mechanical behavior is similar to actual [12, 30].

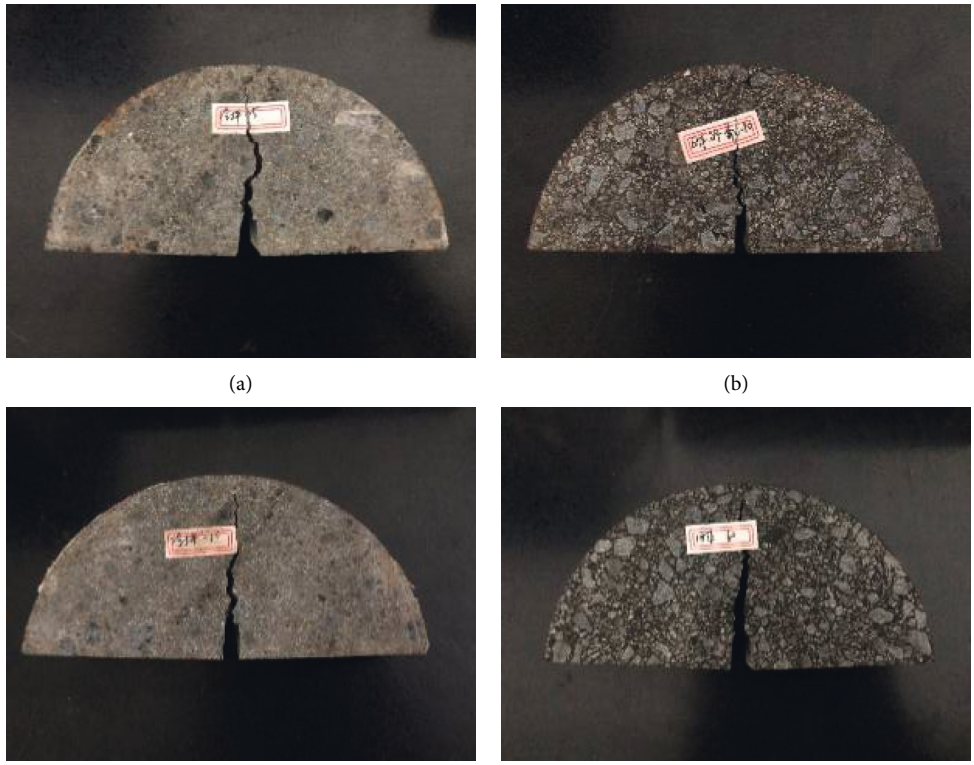

(a) (b) (c) (d)

Figure 11: Failure states of (a) CME concrete @25°C, (b) HEMA concrete @25°C, (c) CME concrete @60°C, and (d) HEMA concrete @60°C after SCB test.

Table 15: Parameters determined from semicircular bending test.

Type	T (°C)	Displacement (mm)	Peak load (kN)	W_f (J)	G_f (J/m^2)
CME concrete	25	2.852	11.581	6.20	2068
	60	2.476	3.289	2.66	888
HMEA concrete	25	2.354	11.352	6.82	2273
	60	2.758	3.328	2.86	952

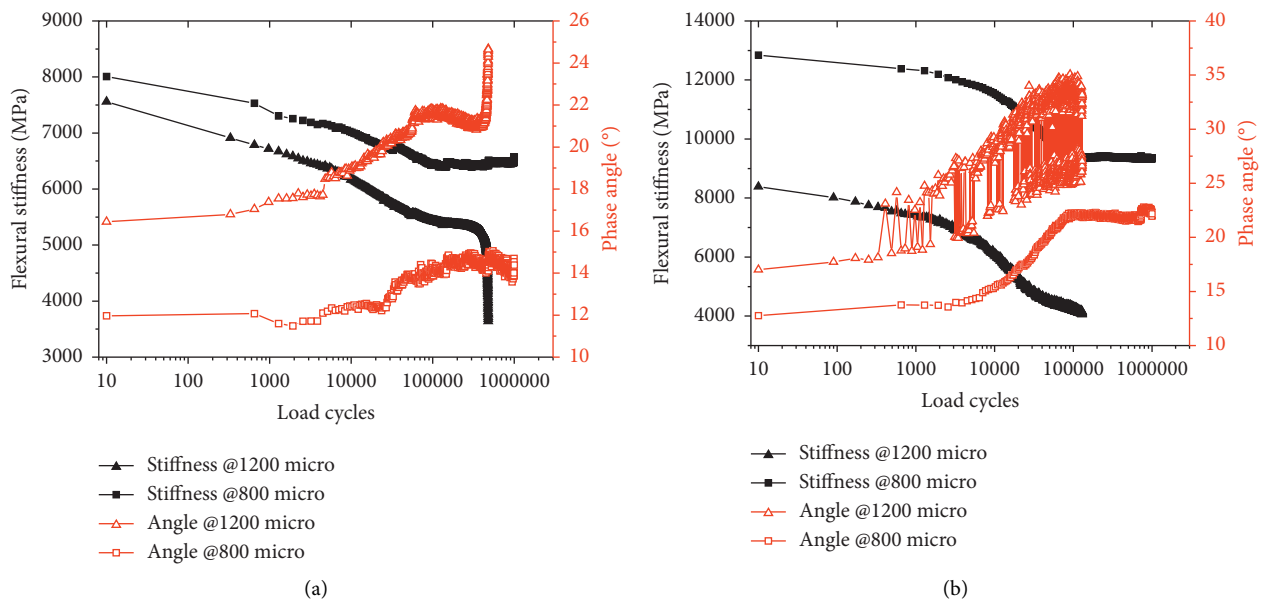

Figure 12: Flexural stiffness and phase angle versus load cycles. (a) CME concrete and (b) HMEA concrete.

Table 16: The four-point beam fatigue behavior of CME concrete and HMEA concrete.

Type	Strain level (micro)	Loading cycles	Initial stiffness (MPa)	Residual stiffness (%)	Cumulative dissipated energy (MJ/m^3)	Initial phase angle (deg)	Finial phase angle (deg)
CME concrete	1200	481700	7253	50.0	4211.0	16.2	24.6
	800	1000000	7870	83.4	3220.6	12.0	14.4
HMEA concrete	1200	129610	8129	50.0	1345.9	17.5	33.2
	800	1000000	12635	73.9	7041.3	12.9	22.2

Figure 12shows the flexural stiffness versus load cycles with different load strain levels. The specific values of four-point beam fatigue of CME concrete and HMEA concrete are shown in Table 16. It was observed apparently that the flexural stiffness decreased with an increase in load cycles. This trend is similar to the fatigue behavior of asphalt concrete [39]. Furthermore, the degree of flexural stiffness decline is associated with load strain level, the higher load strain level, and the faster flexural stiffness decline rate. The results of the fatigue behavior of asphalt concrete indicated that a higher load strain level usually causes faster fatigue damage at each load cycle and a shorter fatigue life [40].

In steel deck pavement, an ideal pavement is required that the fatigue life is greater than 1 million times when the strain level is constant to 400 micro. Under the low strain level (<400 micro), the pavement fatigue life is always greater than 1 million times, it's impossible to know the complete fatigue performance between various steel deck pavements. Recently, some researchers [11, 29, 33] tested the fatigue life of steel deck pavement at a high strain level (>600 micro) and the residual ratio of flexural stiffness was used to evaluate the fatigue behavior.

When the load strain level is constant at 800 micro, the flexural stiffness of CME concrete is still very high after 1 million load cycles, while the residual flexural stiffness of HMEA concrete is 73.9% after 1 million load cycles. When the load strain level rises from 800 micro to 1200 micro, the flexural stiffness of CME concrete and HMEA concrete all drops rapidly and a noticeable transition zone can be observed which means some damage occurs. For linear elastic materials, there is no relationship between the strain level and the flexural stiffness. However, it was found that there was a slight difference among the initial stiffness at different strain levels, indicating that the CME and HMEA are not linear elastic materials.

Unlike the flexural stiffness, there are limited research studies about phase angle during fatigue testing of epoxy asphalt concrete, while the phase angle has been widely reported in dynamic modulus testing of epoxy asphalt concrete [22, 25, 27]. Figure 12 shows the phase angle versus load cycles with different load strain levels. It was observed apparently that the phase angle increased with an increase in load cycle. Furthermore, the degree of phase angle growth is associated with load strain level, the higher load strain level, the faster phase angle growth rate. In addition, it was found that when the flexural stiffness was rapidly reduced, the phase angle rapidly increased. As the load cycle gradually increased, the phase difference between the strain and stress increases, and the viscoelastic properties of the materials become more and more obvious. For HMEA concrete, the phase angle fluctuates seriously when the load strain increases from 800 micro to 1200 micro, which means that some damage occurs with the load cycle.

4. Conclusions

The purpose of this paper was to comprehensively evaluate the novel CME concrete used for steel deck pavement, with HMEA concrete as a comparison. From the experimental results, the following conclusions can be drawn:

(1) The activation energy and the curing reaction order calculated by DSC can be used to evaluate the curing behavior of epoxy-based materials used in steel deck pavement. While the CME is mixed at room temperature and the HME is mixed at 170°C, the curing reaction order of the CME is similar to that of HME and the activation energy of CME is slightly higher than HME.

(2) The damping behavior calculated by DMA can be used to quantitatively evaluate the mechanical properties over a wide temperature range. The peak of tanδ occurs at a low temperature means that the CME and HMEA all have good damping behavior.

(3) The impact toughness calculated by the three-point bending test and the fracture energy determined by the semicircular bending test can reflect the crack resistance of the steel deck pavement at low temperature (such as −10°C) and high temperature (such as 60°C), respectively. CME concrete has a better crack resistance than HMEA concrete at low temperature, and a similar crack resistance compared to HMEA concrete at high temperature.

(4) The residual flexural stiffness ratio after 1 million load cycles can be used as a key parameter to evaluate the fatigue behavior of epoxy-based materials in steel deck pavement, and the CME concrete shows a better fatigue resistance than HMEA concrete.

Data Availability

Some or all data that support the findings of this study are available from the corresponding author (xiejg@nuaa.edu.cn) and first author (likuan901228@163.com) upon reasonable request.

Conflicts of Interest

The authors declare that they have no known competing financial interests or personal relationships that could have appeared to influence the work reported in this paper.

Acknowledgments

This study was supported by the Natural Science Foundation of Jiangsu Province (BK20181112 and BK20180113). Also, the authors of the following references are appreciated.

References

[1] Q. Lu and J. Bors, "Alternate uses of epoxy asphalt on bridge decks and roadways," *Construction and Building Materials*, vol. 78, pp. 18–25, 2015.

[2] C. Wang, Y. Fu, Q. Chen, B. Chen, and L. Zhou, "Application and research advances in epoxy asphalt concrete serving as deck pavement material," *Material", Materials Review*, vol. 32, pp. 2992–3009, 2018.

[3] C. Wang, Q. Chen, Z. Gao, T. Jiang, and J. Chen, "Review on status and development of gussasphalt concrete," *Materials Review*, vol. 31, pp. 135–145, 2017.

[4] S. Luo, Z. M. Liu, X. Yang, Q. Lu, and J. Yin, "Construction technology of warm and hot mix epoxy asphalt paving for long-span steel bridge," *Journal of Construction Engineering and Management*, vol. 145, no. 12, Article ID 04019074, 2019.

[5] W. Huang, W. Q. Guo, and Y. Wei, "Thermal effect on rheological properties of epoxy asphalt mixture and stress prediction for bridge deck paving," *Journal of Materials in Civil Engineering*, vol. 31, no. 10, Article ID 4259505, 2019.

[6] Z. D. Qian, Y. Liu, C. B. Liu, and D. Zheng, "Design and skid resistance evaluation of skeleton-dense epoxy asphalt mixture for steel bridge deck pavement," *Construction and Building Materials*, vol. 114, pp. 851–863, 2016.

[7] W. Huang, Z. D. Qian, G. Chen, and J. Yang, "Epoxy asphalt concrete paving on the deck of long-span steel bridges," *Chinese Science Bulletin*, vol. 48, no. 21, pp. 2391–2394, 2003.

[8] K. Li, Y. Pan, H. Zhang, L. Chen, and J. Zhang, "Research progress of compatibility of epoxy asphalt for steel deck pavement," *Materials Review*, vol. 32, pp. 1534–1540, 2018.

[9] W. Q. Wang and H. Y. He, "Study on performance of epoxy asphalt concrete applied in the deck pavement of pingsheng steel bridge," *Advanced Materials Research*, vol. 150-151, pp. 470–474, 2010.

[10] C. Zhu, "Japan TAF epoxy asphalt concrete design and steel bridge deck pavement construction technology," *Applied Mechanics and Materials*, vol. 330, pp. 905–910, 2013.

[11] Z. Wang and S. Zhang, "Fatigue endurance limit of epoxy asphalt concrete pavement on the deck of long-span steel bridge," *International Journal of Pavement Research and Technology*, vol. 11, no. 4, pp. 408–415, 2018.

[12] Y. M. Yang, Z. D. Qian, and X. Song, "A pothole patching material for epoxy asphalt pavement on steel bridges: fatigue test and numerical analysis," *Construction and Building Materials*, vol. 94, pp. 299–305, 2015.

[13] R. Chen, J. Gong, Y. J. Jiang, Q. J. Wang, Z. H. Xi, and H. F. Xie, "Halogen-free flame retarded cold-mix epoxy asphalt binders: rheological, thermal and mechanical characterization," *Construction and Building Materials*, vol. 186, pp. 863–870, 2018.

[14] J. J. Si, Z. X. Jia, J. Y. Wang et al., "Comparative analysis of cold-mixed epoxy and epoxy SBS-modified asphalts: curing rheology, thermal, and mechanical properties," *Construction and Building Materials*, vol. 176, pp. 165–171, 2018.

[15] J. J. Si, Y. Li, and X. Yu, "Curing behavior and mechanical properties of an eco-friendly cold-mixed epoxy asphalt," *Materials and Structures*, vol. 52, no. 4, p. 81, 2019.

[16] H. Zhang, P. Gao, Y. Pan, K. Li, Z. Zhang, and F. Geng, "Development of cold-mix high-toughness resin and experimental research into its performance in a steel deck pavement," *Construction and Building Materials*, vol. 235, Article ID 117427, 2020.

[17] P. L. Cong, S. F. Chen, and J. Y. Yu, "Investigation of the properties of epoxy resin-modified asphalt mixtures for application to orthotropic bridge decks," *Journal of Applied Polymer Science*, vol. 121, no. 4, pp. 2310–2316, 2011.

[18] Z. D. Qian, L. L. Chen, Y. Q. Wang, and J. L. Shen, "Curing reaction model of epoxy asphalt binder," *Journal of Wuhan University of Technology-Materials Science Edition*, vol. 27, no. 4, pp. 763–767, 2012.

[19] H. Y. Yin, H. Jin, C. S. Wang et al., "Thermal, damping, and mechanical properties of thermosetting epoxy-modified asphalts," *Journal of Thermal Analysis and Calorimetry*, vol. 115, no. 2, pp. 1073–1080, 2014.

[20] H. Y. Yin, Y. G. Zhang, Y. Sun et al., "Performance of hot mix epoxy asphalt binder and its concrete," *Materials and Structures*, vol. 48, no. 11, pp. 3825–3835, 2015.

[21] P. Apostolidis, X. Y. Liu, M. van de Ven, S. Erkens, and T. Scarpas, "Kinetic viscoelasticity of crosslinking epoxy asphalt," *Transportation Research Record*, vol. 2673, no. 3, pp. 551–560, 2019.

[22] G. D. Zeng, W. Xu, H. M. Huang, and X. N. Zhang, "Study on the microstructure and properties of hot-mix epoxy asphalt," *International Journal of Pavement Research and Technology*, vol. 12, no. 2, pp. 147–153, 2019.

[23] Y. Xiao, M. F. C. van de Ven, A. A. A. Molenaar, Z. Su, and F. Zandvoort, "Characteristics of two-component epoxy modified bitumen," *Materials and Structures*, vol. 44, no. 3, pp. 611–622, 2011.

[24] Y. Xiao, M. F. C. van de Ven, A. A. A. Molenaar, Z. Su, and K. Chang, "Design approach for epoxy modified bitumen to be used in antiskid surfaces on asphalt pavement," *Construction and Building Materials*, vol. 41, pp. 516–525, 2013.

[25] L. Chen and Z. Qian, "Study on dynamic modulus of epoxy asphalt mixture based on simple performance test," *Journal of Building Materials*, vol. 16, pp. 341–344, 2013.

[26] B. Yao, G. Cheng, X. Wang, and C. Cheng, "Characterization of the stiffness of asphalt surfacing materials on orthotropic steel bridge decks using dynamic modulus test and flexural beam test," *Construction and Building Materials*, vol. 44, pp. 200–206, 2013.

[27] B. Yao, G. Cheng, X. Wang, C. Cheng, and S. Y. Liu, "Linear viscoelastic behaviour of thermosetting epoxy asphalt concrete - experiments and modeling," *Construction and Building Materials*, vol. 48, pp. 540–547, 2013.

[28] Y. C. Xue and Z. D. Qian, "Development and performance evaluation of epoxy asphalt concrete modified with mineral fiber," *Construction and Building Materials*, vol. 102, pp. 378–383, 2016.

[29] S. Luo, Z. D. Qian, X. Yang, and Q. Lu, "Fatigue behavior of epoxy asphalt concrete and its moisture susceptibility from flexural stiffness and phase angle," *Construction and Building Materials*, vol. 145, pp. 506–517, 2017.

[30] S. Luo, Z. Qian, and J. Harvey, "Experiment on fatigue damage characteristics of epoxy asphalt mixture," *China Journal of Highway and Transport*, vol. 26, pp. 20–25, 2013.

[31] P. L. Cong, W. H. Luo, P. J. Xu, and Y. H. Zhang, "Chemical and physical properties of hot mixing epoxy asphalt binders," *Construction and Building Materials*, vol. 198, pp. 1–9, 2019.

[32] J. Y. Yu, P. L. Cong, S. P. Wu, and S. B. Cheng, "Curing behavior of epoxy asphalt," *Journal of Wuhan University of Technology-Materials Science Edition*, vol. 24, no. 3, pp. 462–465, 2009.

[33] S. Zhang, X. Zhang, W. Xu, Z. Hao, and C. Wan, "Epoxy asphalt concrete fatigue performance design for a steel bridge deck pavement based on impact toughness," *Journal of Vibration and Shock*, vol. 32, pp. 1–5, 2013.

[34] I. R. Henriques, L. A. Borges, M. F. Costa, B. G. Soares, and D. A. Castello, "Comparisons of complex modulus provided by different DMA," *Polymer Testing*, vol. 72, pp. 394–406, 2018.

[35] A. J. Hanz, A. Faheem, E. Mahmoud, and H. U. Bahia, "Measuring effects of warm-mix additives use of newly developed asphalt binder lubricity test for the dynamic shear rheometer," *Transportation Research Record*, vol. 2180, no. 1, pp. 85–92, 2010.

[36] Y. Xue, S. Wu, J. Cai, M. Zhou, and J. Zha, "Effects of two biomass ashes on asphalt binder: dynamic shear rheological characteristic analysis," *Construction and Building Materials*, vol. 56, pp. 7–15, 2014.

[37] Y. Kang, M. Song, L. Pu, and T. Liu, "Rheological behaviors of epoxy asphalt binder in comparison of base asphalt binder and SBS modified asphalt binder," *Construction and Building Materials*, vol. 76, pp. 343–350, 2015.

[38] Y. Chen, N. Hossiney, X. Yang, H. Wang, and Z. You, "Application of epoxy-asphalt composite in asphalt paving industry: a review with emphasis on physicochemical properties and pavement performances," *Advances in Materials Science and Engineering*, vol. 2021, Article ID 3454029, 35 pages, 2021.

[39] J. L. L. Júnior, L. F. A. L. Babadopulos, and J. B. Soares, "Moisture-induced damage resistance, stiffness and fatigue life of asphalt mixtures with different aggregate-binder adhesion properties," *Construction and Building Materials*, vol. 216, pp. 166–175, 2019.

[40] T. M. Ahmed, H. Al-Khalid, and T. Y. Ahmed, "Review of techniques, approaches and criteria of hot-mix asphalt fatigue," *Journal of Materials in Civil Engineering*, vol. 31, no. 12, Article ID 03119004, 2019.